Synthetic homeostatic materials with chemo-mechano-chemical self-regulation

Synthetic Homeostatic Materials Displaying Chemo-mechano-chemical Self-regulation

*Ximin He,[1,2] Michael Aizenberg,[2] Olga Kuksenok,[3] Lauren D. Zarzar,[4] Ankita Shastri,[4] Anna Balazs,[3] Joanna Aizenberg[1,2,4]**

[1]School of Engineering and Applied Sciences, Harvard University, Cambridge, Massachusetts 02138, USA; [2]Wyss Institute for Biologically Inspired Engineering, Harvard University, Cambridge, Massachusetts 02138, USA; [3]Department of Chemical and Petroleum Engineering, University of Pittsburgh, Pittsburgh, Pennsylvania 15260, USA; [4]Department of Chemistry and Chemical Biology, Harvard University, Cambridge, Massachusetts 02138, USA

*To whom correspondence should be addressed. Email: jaiz@seas.harvard.edu

Living organisms exhibit unique homeostatic abilities, maintaining tight control of their local environment through inter-conversions of chemical and mechanical energy and self-regulating feedback loops organized hierarchically across many length scales[1-7]. In contrast, most synthetic materials are incapable of undergoing continuous self-monitoring and self-regulating behavior due to their limited single-directional chemo-mechanical[7-12] or mechano-chemical[13, 14] modes. Applying the concept of homeostasis to the design of autonomous materials[15] would have transformative impacts in areas ranging from medical implants that help stabilize bodily functions to smart materials that regulate energy usage[2, 16, 17]. Here we present a versatile strategy for creating self-regulating, self-powered, homeostatic materials capable of precisely tailored chemo-mechano-chemical feedback loops at the nano/microscale. We design a bilayer system with hydrogel-supported, catalyst-bearing microstructures, which are separated from a reactant-containing "nutrient" layer. Reconfiguration of the gel in response to a stimulus induces the reversible actuation of the microstructures in and out of the nutrient layer and serves as a highly precise "on/off" switch for chemical reactions. We apply this design to trigger organic, inorganic and biochemical reactions that undergo reversible, repeatable cycles synchronized with the motion of the microstructures and the driving external chemical stimulus. By exploiting a continuous feedback loop between various exothermic catalytic reactions in the nutrient layer and the mechanical action of the temperature-responsive gel, we then create exemplary autonomous, self-sustained homeostatic systems that maintain a user-defined parameter—temperature—in a narrow range. The experimental results were validated using computational modeling that qualitatively captured the essential features of the self-regulating behavior and provided additional criteria for the optimization of the homeostatic function, subsequently confirmed experimentally. This design is highly customizable due to the broad choice of chemistries, tunable mechanics, and physical simplicity, thus promising exciting applications in autonomous systems with chemo-mechano-chemical transduction at their core.

The survival of organisms relies on homeostatic functions such as the maintenance of stable body temperature, blood pressure, pH, and sugar levels[1, 3, 5-7]. This remarkable self-

regulatory capability can be traced to macromolecular components that convert chemical processes into nano/microscale motion and vice versa, such as ATP synthesis[5] and muscle contraction[4, 7], thereby mechanically-mediating the coupling of a wide range of disparate chemical signals[1, 2]. Despite its importance in living systems, the concept of homeostasis and self-regulation has not been applied extensively to man-made materials, leaving many to be energy inefficient or to fail in the face of minor perturbations. Synthetic materials typically only sense or actuate along a single chemo-mechanical (C→M)[8-12] or mechano-chemical (M→C)[13, 14] route and are generally incapable of integration into feedback mechanisms that necessarily incorporate both pathways (C_1→M→C_2 or C⇄M). There are a few stimuli-responsive drug delivery systems, which utilize chemo-mechano-chemical elements that lead to release of certain molecules to target locations[18-20]. Select oscillating and non-oscillating reactions have been coupled to reversible mechanical responses[21-25], yet systems that are driven by such a limited chemical repertoire lack versatility and tunability. Despite substantial efforts, artificial chemo-mechanical systems capable of integration within hierarchical regimes, taking advantage of compartmentalization and partition[26], offering smooth coupling of microscopic and macroscopic signals with fast mechanical action[4] and a wide range of chemical inputs and outputs remain a highly desired but elusive goal[16, 17]. In response to these challenges, we describe here a new materials platform that can be designed to mediate a variety of homeostatic feedback loops. The system, which we call SMARTS (Self-regulated Mechano-chemical Adaptively Reconfigurable Tunable System), reversibly transduces external or internal chemical inputs into user-defined chemical outputs via the "on/off" mechanical actuation of microstructures.

The general, customizable design of SMARTS is presented in Fig.1a. Partially embedded in a hydrogel "muscle", high-aspect-ratio "skeletal" microstructures with a catalyst or reagent affixed to the tips reversibly actuate as the gel swells/contracts in response to a chemical stimulus (C_1). When this system is immersed in a liquid bilayer, this mechanical action (M) moves the catalyst into and out of a top "nutrient" layer of reactants, such that a chemical reaction (C_2) is turned on when the microstructures straighten and turned off when they bend, realizing a synchronized cascade of chemo-mechanical energy inter-conversions (C_1→M→C_2). We built such a system using an epoxy microfin array (Fig.1b) that reconfigures between upright and bent states (Fig.1c) upon hydrogel volume change. The catalyst or reagent of choice was physically adsorbed or chemically attached to the tips of the microstructures (Fig.1d, Fig.S1,

Supplementary Information (SI)). The formation of a stable bilayer configuration was achieved in either a biphasic system or in a microfluidic device (Fig.S2, SI) and the position of the interface was determined by confocal microscopy using fluorescently labeled liquids (Fig.1e).

Using this design, we first characterized and optimized a number of externally regulated $C_1 \rightarrow M \rightarrow C_2$ systems which show that SMARTS can be tailored for a broad range of coupled chemo-mechanical and mechano-chemical events (Fig.2). We incorporated microstructures actuated by a pH-responsive hydrogel, poly(acrylamide-*co*-acrylic acid)[27], into a microfluidic channel[28] and utilized laminar flow to generate atop the microstructured surface a stable liquid bilayer (Fig.S2). Using periodic changes in pH in the bottom layer as the stimulus S, we realized chemo-mechano-chemical cycles of the type $(S_{on} \rightarrow C_1 \rightarrow M_{up} \rightarrow C_2) \rightarrow (S_{off} \rightarrow C_{-1} \rightarrow M_{bent} \not\rightarrow C_2) \rightarrow (S_{on} \rightarrow \ldots)$, where S_{on} and S_{off} correspond to pH change; C_1 and C_{-1} denote deprotonation of the acrylic acid and protonation of the acrylate moieties, respectively; M_{up} and M_{bent} denote the movement of the microstructures between the two liquid layers, and C_2 denotes various reactions triggered in the top layer (Fig.2).

To determine optimal conditions allowing the microstructures to pass sufficiently far across the fluidic interface (Fig.2a,b), we applied fluorescein onto the microstructure tips and observed the "on/off" states of fluorescein quenching by potassium iodide in the upper, "nutrient" layer. By tracking the progress of both the chemical reaction and the motion of the microstructures (Fig.2c, Fig.S3), we demonstrated that the quenching started at almost the exact moment the 18-μm-tall tips crossed the ~12-μm-high interface into the layer of reagents, and ceased as the tips crossed again upon leaving the KI solution. The high level of chemo-mechanical coordination of SMARTS therefore provides a precise and controllable way to use mechanical action to alter and affect dynamics of chemical systems and a basis for the design of far more complex, compartmentalized[2, 16, 17, 26] chemo-mechano-chemical interactions.

Not only is this mechanical mediation inherently precise, but the system response is also fast, allowing for rapid switching of an induced chemical reaction. We demonstrated, for example, that the pulsed generation of O_2 gas bubbles (~35 $nL \cdot mm^{-2} \cdot s^{-1}$) by a Pt-catalyzed hydrogen peroxide decomposition reaction, $2H_2O_2 \xrightarrow{Pt} O_2 + 2H_2O$ (Fig.2d-f, Movie 1, Fig.S4) can be switched on and off entirely within a fraction of a second, in synchrony with the driving chemical stimulus. This system can also be designed to regulate far more complex,

multicomponent enzymatic processes occurring in delicate biologically-relevant conditions. The variety of switchable C_2 reactions is complemented by the customizability of the hydrogel response, which can be tailored to a wide range of stimuli, such as pH, heat, light, glucose or other metabolic compounds, allowing one to mix and match chemical signals at will.

Of particular interest and potential importance is the ability to design *self-regulated, autonomous* $C_1 \rightarrow M \rightarrow C_2$ systems in which the chemical output signal is matched with the stimulus of the responsive hydrogel. Such a system would show homeostatic behavior due to the possibility of a complete, continuous feedback loop, $C \rightarrow M \rightarrow C \rightarrow M \rightarrow \ldots$ or $C \rightleftarrows M$ (Fig.3a). Here we demonstrated this unique capacity by creating multiple self-powered, self-regulated oscillating systems via coupling the mechanical action of a temperature-responsive gel, poly(*N*-isopropylacrylamide) (pNIPAAm), with several exemplary exothermic catalytic reactions:

(i) hydrosilylation of 1-hexene with triethylsilane catalyzed by H_2PtCl_6

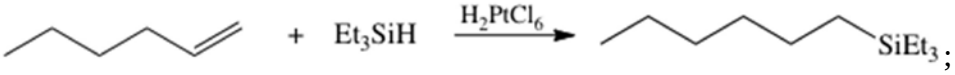

(ii) hydrosilylation of 1-hexene with diphenylsilane catalyzed by H_2PtCl_6

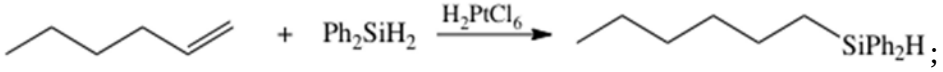

(iii) decomposition of cumene hydroperoxide catalyzed by Ph_3CPF_6

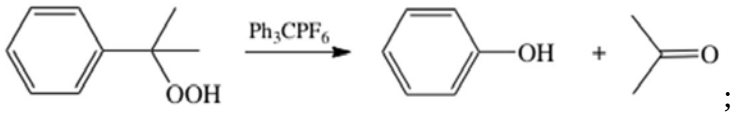

(iv) "click" reaction between octylazide and phenylacetylene catalyzed by $Cu(PPh_3)_2NO_3$

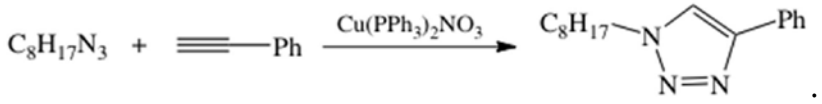

Below the lower critical solution temperature (LCST), the thermally-responsive hydrogel swells, the embedded microstructures straighten, and their catalyst-functionalized tips enter the reagent layer, triggering an exothermic reaction; when the temperature increases to T>LCST due to the generated heat, it triggers contraction of the hydrogel, removing the microstructures from the reagents; when the temperature falls to T<LCST again, the cycle restarts, giving rise to continuous, self-regulated $C \rightleftarrows M$ oscillations (Fig.3a). All these systems behave as remarkable autonomous thermal regulators that maintain within a very narrow range the local temperature,

which is determined by the LCST of the hydrogel (Fig.3b). For example, when pNIPAAm hydrogel (LCST=32.0°C)[29] was used to switch reaction (i), the local temperature fluctuated between 31.0-33.8°C (Fig.3c, Fig.S5). When we modified the pNIPAAm with 5% butyl methacrylate[30], in order to reduce the LCST to 27.8°C, the stabilized temperature range shifted to 27.1-29.7°C (Fig.3c,d). This robust self-contained feedback system, which is <70-μm-thick, regulates the temperature of a 0.64 cm^2 surface for ~6 h (4.20 min/cycle for 95 cycles) with an initial input of only 4.0 μL of reactants as fuel (Movie 2); with periodic replenishment of reactants it can continue to function almost indefinitely. The oscillation amplitude and period vary depending on the reactions' exothermicity and kinetics (see discussion below and Fig.S6-8).

To capture essential features of the self-regulating, oscillatory behavior seen in the experiments and assess the contributions of different variables, we developed a novel hybrid computational approach to model microstructures that are embedded in a thermo-responsive gel and interact with an overlaying layer of reagents (Fig.S9, SI). This approach is based on the gel lattice spring model (gLSM)[31-33] to describe the elastodynamics of the gel layer (Fig.4a). Simulations show that the phase trajectory of the z-coordinate of the microstructure tips, $z_{tip}(T)$ (Fig.4b), develops into a stable limit cycle, corresponding to robust, self-sustained oscillations (Fig.4c). By focusing on a single oscillation cycle (Fig.4d), we see that in agreement with the experiments (Fig.3c), the temperature of the system decreases when the tips are below the bilayer interface and increases when they are above this plane, resulting in a phase shift (about 1/3 oscillation period) between the oscillations in temperature and tip position. Furthermore, at any temperature *T* within the oscillation cycle, z_{tip} can attain one of two possible values, so that at the same *T*, the tips are higher during the heating and lower during the cooling, as marked by $z_{tip}^{heat}(T^*) > z_{tip}^{cool}(T^*)$ in Fig.4d (the same behavior is also observed in experiments as seen in Fig. 3d). The latter feature is also clearly evident from Fig.4b, where the upper portion of the limit cycle corresponds to the tips located above the interface (above the green line) and to the increase in *T* (marked by the red arrow pointing to the right) and the lower portion corresponds to the tips located below the interface and to the decrease in *T* (marked by the red arrow pointing to the left). The bistability seen in Fig.4d, as well as the negative feedback provided by the localized reaction, results in the oscillations seen in Figs.3,4. Notably, bistability has been shown to play a key role in various self-oscillating gels[21, 22]; for example, bistability in the permeability

of a gel membrane[21, 22] or spatial bistability in pH-responsive gels[21, 22] results in distinct chemo-mechanical oscillations.

Importantly, our model provides predictive abilities for estimating the trends in homeostatic behavior based on tunable variables. For example, the modeling suggested (SI, Fig.S10) that the homeostatic temperature and oscillation amplitude could be controlled by varying the liquid-liquid interface position, geometry/mechanical properties of the microstructures, and heating rate. The predicted trends were further confirmed by detailed experiments. Specifically we note that the oscillation period gradually increases as the reactions progress; while the average period in reaction (i) was 4.20 min/cycle (Fig.3c), it increased from the initial value of 3.58 to 4.50 min/cycle as reactants were depleted (Fig.S5c). Such an increase is in agreement with the predicted effect of varying the heating rate (Fig.S10c), which depends on the reaction exothermicity and the reactant concentration. To study this effect further, we performed the hydrosilylation reaction with diluted reagents (80% vol./vol.) and observed, as predicted, the increase of the initial oscillation period to 3.85 min/cycle, as well as the decrease of the amplitudes of both temperature (2.3°C vs 2.8°C) and tip position (~3 μm vs ~4 μm), as shown in Fig.S6a. In contrast, when a more reactive diphenylsilane was used in place of triethylsilane, the higher heating rate resulting from a more vigorous reaction led to a shorter oscillation period (3.20 min/cycle) and larger amplitudes of both temperature (5.0°C) and tip position (~7 μm) (Fig.S6a). Similar results were obtained for SMARTS using other types of exothermic reactions (see reactions (iii) and (iv)) (Fig.S6b).

To study the correlation of the homeostatic performance and position of the liquid interface, we raised the bilayer interface from ~12 μm to ~15 μm. With the higher interface, the microfins oscillated with a smaller amplitude of ~2 μm (vs ~4 μm) (Fig.S7a). The temperature fluctuations were dampened as well (the new amplitude of 1.7°C vs 3.2°C), around a slightly lower homeostatic point (32.0°C compared to the original homeostatic point of ~32.7°C), conceivably due to the fact that the catalyst-coated microstructure tips remain in the reagent layer for shorter amounts of time when the interface is higher. All the latter effects of varying the interface position are also observed in our simulations (SI, Fig.S10a,b). To study the correlation of the homeostatic performance and microstructure size, 14.5-μm-tall microfins were used instead of the original 18.0-μm-tall ones. Reducing the fin height, while keeping the position of the liquid interface constant, resulted in the expected increase of the initial oscillation period

(3.80 min/cycle) and the decrease of the actuation amplitude (to ~2 μm around a lower level of ~11 μm). At the same time, the temperature fluctuation amplitude increased to 5.0°C (between 30.2-35.2°C) (Fig.S7b).

In summary, we have developed a self-regulated, adaptively reconfigurable, tunable system (SMARTS) that shows unique homeostatic function based on coupled chemo-thermo-mechanical self-oscillations. Our studies not only unravel SMARTS dynamic and collective responsiveness and the highly complex non-equilibrium behavior that typifies the C⇄M transitions, but also provide criteria for optimization and customization of its design. We have demonstrated that the homeostatic temperature can be controlled by the LCST of the responsive gel; the frequency and amplitude of the autonomous temperature oscillation depend on the chemical reaction used and, for a given reaction, they can be finely tuned by adjusting the liquid interface height, heat generation rate via controlled reagent concentration, or microstructures dimension/geometry. We anticipate that the ability of SMARTS to maintain a stable temperature can be used in autonomous self-sustained thermostats for applications ranging from medical implants that help stabilize bodily functions to smart buildings that regulate thermal flow for increased energy efficiency. In general, our rich SMARTS platform can involve a variety of other stimuli-responsive gels and catalytic reactions, enabling the creation of diverse homeostatic systems with various regulatory functions (including pH, light, glucose, pressure, *etc.*). An oscillating mechanical movement originating from a non-oscillatory source, leading to autonomous motility, has considerable potential for translation into areas such as robotics, biomedical engineering, microsystems technology, architecture, to name just a few. The system also can be applied for sensing and sorting of analytes in a microreactor device. The micrometer length scale, customizability, and physical simplicity of SMARTS allow it to be integrated with other microscale devices, leading to far more complex self-powered, continuous or pulsed hierarchical chemo-mechanical systems capable of maintaining local state conditions.

Methods summary

SMARTS fabrication: Microfins were made by polymerizing epoxy resin (UVO-114 with 10% by weight glycidyl methacrylate) within PDMS molds that were replicated from Si masters with corresponding geometry. Microfins were partially embedded in hydrogel by depositing an

appropriate amount of hydrogel precursor solution on the microfins-bearing epoxy substrates and curing under UV illumination. Microstructure tips were functionalized by stamping with a flat PDMS sheet inked with catalysts or fluorescence dye followed by thorough rinsing. To create a bilayer of aqueous liquids on top of the sample, the sample was integrated in a microfluidic device. Channels were laser cut into acrylic double-sided adhesive sheets and placed on top of the sample, and the channels were capped with PDMS allowing integration with polyethylene tubing, creating two inlets connected to two syringe pumps and an outlet. The height of the aqueous/aqueous interface was adjusted by changing the flow rates of the two ingoing solutions. To create a bilayer of organic/aqueous liquid, the two solutions of fixed volumes were sequentially placed on top of the microfins, forming a stable interface at a fixed height.

SMARTS characterization: Confocal microscopy was used to determine the position of the liquid interface and tip positions of the actuating microfins. Optical imaging and video recording were done on an inverted microscope. Time-resolved temperature-monitoring of SMARTS with incorporated exothermic reactions was carried out by precision fine wire thermocouples connected to a temperature controller and a computer.

Simulations: The gel lattice spring model (gLSM)[31-33] was extended to encompass elastic filaments that are anchored within a thermo-responsive gel. We account for heat produced by the exothermic reaction when the filament tips are above the reaction plane, as well as the heat dissipation throughout the system.

References

1. Bao, G. et al. Molecular Biomechanics: The Molecular Basis of How Forces Regulate Cellular Function. *Cell. Mol. Bioeng.* **3**, 91-105 (2010).
2. Fratzl, P. & Barth, F.G. Biomaterial systems for mechanosensing and actuation. *Nature* **462**, 442-448 (2009).
3. Guyton, A.C. & Hall, J.E. Human physiology and mechanisms of disease, Edn. 6th. (Saunders, Philadelphia; 1997).
4. Prosser, B.L., Ward, C.W. & Lederer, W.J. X-ROS Signaling: Rapid Mechano-Chemo Transduction in Heart. *Science* **333**, 1440-1445 (2011).
5. Sambongi, Y. et al. Mechanical rotation of the c subunit oligomer in ATP synthase (F0F1): Direct observation. *Science* **286**, 1722-1724 (1999).
6. Spaet, T.H. Analytical Review: Hemostatic Homeostasis. *Blood* **28**, 112-123 (1966).
7. Hess, H. Engineering Applications of Biomolecular Motors. *Annu. Rev. Biomed. Eng.* **13**, 429-450 (2011).

8. Fritz, J. et al. Translating biomolecular recognition into nanomechanics. *Science* **288**, 316-318 (2000).
9. Lahann, J. & Langer, R. Smart materials with dynamically controllable surfaces. *MRS Bull.* **30**, 185-188 (2005).
10. Li, D.B. et al. Molecular, Supramolecular, and Macromolecular Motors and Artificial Muscles. *MRS Bull.* **34**, 671-681 (2009).
11. Paxton, W.F., Sundararajan, S., Mallouk, T.E. & Sen, A. Chemical locomotion. *Angew. Chem. Int. Ed.* **45**, 5420-5429 (2006).
12. Sidorenko, A., Krupenkin, T., Taylor, A., Fratzl, P. & Aizenberg, J. Reversible switching of hydrogel-actuated nanostructures into complex micropatterns. *Science* **315**, 487-490 (2007).
13. Ariga, K., Mori, T. & Hill, J.P. Control of nano/molecular systems by application of macroscopic mechanical stimuli. *Chem. Sci.* **2**, 195-203 (2011).
14. Todres, Z.V. Organic mechanochemistry and its practical applications. (CRC/Taylor & Francis, 2006).
15. Harris, T.J., Seppala, C.T. & Desborough, L.D. A review of performance monitoring and assessment techniques for univariate and multivariate control systems. *J. Process Control* **9**, 1-17 (1999).
16. Stuart, M.A.C. et al. Emerging applications of stimuli-responsive polymer materials. *Nat. Mater.* **9**, 101-113 (2010).
17. Yerushalmi, R., Scherz, A., van der Boom, M.E. & Kraatz, H.B. Stimuli responsive materials: new avenues toward smart organic devices. *J. Mater. Chem.* **15**, 4480-4487 (2005).
18. Das, M., Mardyani, S., Chan, W.C.W. & Kumacheva, E. Biofunctionalized pH-responsive microgels for cancer cell targeting: Rational design. *Adv. Mater.* **18**, 80-83 (2006).
19. Murthy, N. et al. A macromolecular delivery vehicle for protein-based vaccines: Acid-degradable protein-loaded microgels. *Proc. Natl Acad. Sci. USA* **100**, 4995-5000 (2003).
20. Nayak, S., Lee, H., Chmielewski, J. & Lyon, L.A. Folate-mediated cell targeting and cytotoxicity using thermoresponsive microgels. *J. Am. Chem. Soc.* **126**, 10258-10259 (2004).
21. Siegel, R.A. in Chemomechanical Instabilities in Responsive Materials. (eds. P. Borckmans, P.D. Kepper & A.R. Khokhlov) (Springer, 2009).
22. Horvath, J., Szalai, I., Boissonade, J. & De Kepper, P. Oscillatory dynamics induced in a responsive gel by a non-oscillatory chemical reaction: experimental evidence. *Soft Matter* **7**, 8462-8472 (2011).
23. Kovacs, K., Leda, M., Vanag, V.K. & Epstein, I.R. Small-Amplitude and Mixed-Mode pH Oscillations in the Bromate-Sulfite-Ferrocyanide-Aluminum(III) System. *J. Phys. Chem. A* **113**, 146-156 (2009).
24. Maeda, S., Hara, Y., Sakai, T., Yoshida, R. & Hashimoto, S. Self-walking gel. *Adv. Mater.* **19**, 3480-3484 (2007).
25. Vanag, V.K. & Epstein, I.R. Resonance-induced oscillons in a reaction-diffusion system. *Phys. Rev. E* **73** (2006).
26. Koga, S., Williams, D.S., Perriman, A. & Mann, S. Peptide-nucleotide microdroplets as a step towards a membrane-free protocell model. *Nat. Chem.* **3**, 720-724 (2011).

27. Richter, A. et al. Review on hydrogel-based pH sensors and microsensors. *Sensors* **8**, 561-581 (2008).
28. Zarzar, L.D., Kim, P. & Aizenberg, J. Bio-inspired Design of Submerged Hydrogel-Actuated Polymer Microstructures Operating in Response to pH. *Adv. Mater.* **23**, 1442-1446 (2011).
29. Schild, H.G. Poly(n-isopropylacrylamide)-experiment, theory and application. *Prog. Polym. Sci.* **17**, 163-249 (1992).
30. Okano, T., Bae, Y.H., Jacobs, H. & Kim, S.W. Thermally on off switching polymers for drug permeation and release. *J. Controlled Release* **11**, 255-265 (1990).
31. Kuksenok, O., Yashin, V.V. & Balazs, A.C. Three-dimensional model for chemoresponsive polymer gels undergoing the Belousov-Zhabotinsky reaction. *Phys. Rev. E* **78**, 1-16 (2008).
32. Yashin, V.V. & Balazs, A.C. Pattern formation and shape changes in self-oscillating polymer gels. *Science* **314**, 798-801 (2006).
33. Yashin, V.V., Kuksenok, O. & Balazs, A.C. Modeling autonomously oscillating chemo-responsive gels. *Prog. Polym. Sci.* **35**, 155-173 (2010).

Figure legends

Figure 1. General design of SMARTS. a, Cross-section. **b**, 3-D schematic. **c**, Top-view microscope images of upright and bent microfins corresponding to "on/off" reaction states. **d**, 45° side-view (left) and top-view (right) SEM images of 2Wx10Lx18H μm microfins with the catalyst particles on tips (inset). **e**, 3-D confocal microscope image of a hydrogel-embedded 18-μm-tall post array immersed in a bilayer liquid labeled with fluorescein and Rhodamine B revealing the interface height at 12μm (Fig.S2).

Figure 2. Oscillations in exemplary chemical reactions triggered by pH changes. a-c, Fluorescence quenching: **a**, Schematic; **b**, Confocal microscope images showing green fluorescence of fluorescein on the tips of bent fins that disappears as fins enter the quenching KI layer. The red color arises from Rh B in the bottom layer; **c**, Fluorescence intensity as a function of the tip position (Z). No fluorescence quenching occurs in the controls containing no KI in the top layer (Fig.S3). **d-f**, Pulsed Pt-catalyzed H_2O_2 decomposition: **d**, Schematic; **e**, Optical microscope images showing intermittent oxygen bubble generation when the catalyst-bearing tips enter the H_2O_2 layer. The colors arise from pH indicator, bromophenol blue. No bubbles form in the controls without Pt catalyst (Fig.S4); **f**, Time-resolved gas generation synchronous with the actuation of the fins.

Figure 3. Homeostasis in SMARTS via self-regulated chemo-thermo-mechanical feedback loops. a, Schematic of the temperature-regulating SMARTS displaying a C⇄M feedback loop, in which mechanical action of *T*-responsive gel is coupled with an exothermic reaction. The side-view schematic and top-view microscope images depict "on-off" states of the reaction in the top layer. **b,** Temperature oscillations arising from different exothermic reactions driven by *T*-responsive poly(*N*-isopropylacrylamide) gel: (i-ii) Hydrosilylation of 1-hexene with triethylsilane (i) and diphenylsilane (ii); (iii) decomposition of cumene hydroperoxide; (iv) "click" reaction between octylazide and phenylacetylene. **c**, Comparison between temperature oscillations using hydrogels of different LCSTs: 32.0°C (black line) and 27.8°C (red line). The control without catalyst did not maintain *T* and quickly cooled down (Fig.S8). **d**, Time-resolved

temperature and vertical coordinate (Z) of microfin tips for system with LCST of 27.8°C. Note the phase shift between the two curves. Inserts show schematic fin configurations.

Figure 4. Computer simulations of the self-sustained thermal regulation. a, Self-oscillations in SMARTS (microstructures in red, hydrogel in green, bilayer liquid interface marked by the red plane). The color bar indicates the volume fraction of polymer, ϕ, within the hydrogel. **b**, Phase trajectory $z_{tip}(T)$. The system follows the trajectory from left to right (see clockwise arrangement of arrows indicating the time direction). P_1 indicates the tip's initial height at 22°C, and at P_2 the tips first cross the interface. **c-d**, Time evolution of z-coordinate of tips, $z_{tip}(t)$ (blue curve, right axis) and temperature *T(t)* (red curve, left axis); green line marks the position of the interface (red plane in **a**). In **d**, stars mark values $z_{tip}^{heat}(T^*) > z_{tip}^{cool}(T^*)$ and indicate that at fixed *T*, the tips are higher during heating than cooling. In the un-deformed state, the height of the gel layer and posts are 18.6 and 25.6μm respectively, and the dimensionless unit of time corresponds to 4s (SI).

Supplementary Information is linked to the online version of the paper at www.nature.com/nature.

Acknowledgement

We thank Dr. M. Khan for microstructure fabrication; R. S. Friedlander for assistance with confocal imaging; Dr. P. Kim for assistance with the gel formulation; Dr. M. Kolle and Dr. Allen Ehrlicher for technical assistance; Dr. A. Grinthal for help with the manuscript preparation. The work was supported by the DOE under award DE-SC0005247 (experiment) and by the NSF under award CMMI-1124839 (computational modeling).

Author Contribution

X.H., M.A. and J.A. perceived the concepts of the research. J.A. and M.A. supervised the research. X.H. and M.A. designed and conducted the experiments and data analysis. X.H., L.Z. and A.S. conducted the characterization. X.H. and L.Z. carried out microfluidic device design. A.S. carried out hydrogel deposition optimization. O.K. and A.B. developed a model and numerical code and carried out the computational simulations. All authors wrote the manuscript.

Correspondence and requests for materials should be addressed to J.A.